



HAL
open science

Impact of Alternating Fuel Feeding on a PEMFC stack durability

Sandrine Rodosik, Jean-Philippe Poirot, Yann Bultel

► **To cite this version:**

Sandrine Rodosik, Jean-Philippe Poirot, Yann Bultel. Impact of Alternating Fuel Feeding on a PEMFC stack durability. International Journal of Hydrogen Energy, 2021, 46 (79), pp.39415-39426. 10.1016/j.ijhydene.2021.09.154 . cea-03508782

HAL Id: cea-03508782

<https://cea.hal.science/cea-03508782>

Submitted on 5 Jan 2024

HAL is a multi-disciplinary open access archive for the deposit and dissemination of scientific research documents, whether they are published or not. The documents may come from teaching and research institutions in France or abroad, or from public or private research centers.

L'archive ouverte pluridisciplinaire **HAL**, est destinée au dépôt et à la diffusion de documents scientifiques de niveau recherche, publiés ou non, émanant des établissements d'enseignement et de recherche français ou étrangers, des laboratoires publics ou privés.



Distributed under a Creative Commons Attribution - NonCommercial 4.0 International License

Impact of Alternating Fuel Feeding on a PEMFC stack durability

S. Rodosik^{1,2}, J.-P. Poirot-Crouvezier^{1*} and Y. Bultel²

¹*Univ. Grenoble Alpes, CEA, LITEN, DEHT, F-38000 Grenoble, France*

²*Univ. Grenoble Alpes, Univ. Savoie Mont Blanc, CNRS, Grenoble INP, LEPMI, F-38000 Grenoble, France*

***Corresponding author. Univ. Grenoble Alpes, CEA, LITEN, DEHT, F-38000 Grenoble, France.**

E-mail addresses: sandrine.rodosik@cea.fr (S. Rodosik), jean-philippe.poirot@cea.fr (J.-P. Poirot-Crouvezier), yann.bultel@grenoble-inp.fr (Y. Bultel).

Abstract

The integration of PEMFC for transport applications requires cost as well as system complexity reduction. A novel anode circuit architecture named “Alternating Fuel Feeding” (AFF) was developed. It combines on one hand, the benefits of the hydrogen recirculation and on the other hand, the simpleness of Dead-End Anode (DEA). A previous work demonstrated the benefits on the costs and on the anodic line weight. In the present work, investigations on stack durability, from the system scale to the cell scale, are performed during operation in two anode feeding modes: AFF and recirculation. The performances of stacks are evaluated along ageing tests, coupled with local measurements. At the end of life, postmortem analyses are performed on the aged cells. The degradation rates of stack performances are quite similar in both cases while more heterogeneous cell degradation are observed in recirculation mode along with the ageing according to a Fuel Cell Dynamic Load Cycle (FC-DLC).

Keywords

Hydrogen feed strategy, Anode system architecture, Local temperature, Current distribution, Degradation, Automotive conditions.

1. Introduction

Today, Europe through the Fuel Cells and Hydrogen Joint Undertaking (FCH JU) depicts a fuel cell system that is economically viable for transport in light of 2030, with a power density of the stack cells at 10 kW/L, a durability of 7000 h and a production cost of the system lower than 40 €/kW [1].

To achieve these targets, two axes of work are identified: the first one on the reduction of stack volume and mass, and the second one on the systems complexity. According to the US Department of Energy [2,3], the air and hydrogen supply lines influence strongly the complexity of the system and thus its cost. The main function of the anodic fluidic architecture is the control of the flow and the pressure of hydrogen entering the fuel cell, but rarely of its humidification. This can be accomplished by different fluid management strategies and different architectures. The Dead-End Anode (DEA) strategy is the simplest architecture [4–9]. The anodic output valve is kept closed, opening only intermittently to evacuate any species accumulated at the exit of the cell. In DEA, the anode is therefore supplied with dry gas. This causes a drying out of the area close to the hydrogen inlet. This phenomenon, coupled with the accumulation of water and nitrogen at the outlet, induces performance losses [4,8,10–17] as well as irreversible degradations [4,6,18–26]. So, anodic purge strategy is investigated [15,27–33] and often, frequent purges are recommended, inducing hydrogen losses impeding the system efficiency [4,8,10–17,27–33].

The most widespread architecture to our knowledge on systems for the mobility is the recirculation of hydrogen using ejectors [34–37] or recirculation pumps [38–41]. This second configuration allows participating to water management at the anode inlet of the stack. Indeed, the water vapor is recirculated at the anode outlet in order to hydrate the membrane [12,42–47]. A few authors investigated the feasibility to recirculate hydrogen through the stack based on a combination of a specific architecture and a pressure-swing concept [42,48].

Lately, an upgraded anode fluidic architecture, called Alternating Fuel Feeding (AFF), has been proposed at the anode by Rodosik et al. [49]. This latter only requires a new stack configuration and an additional solenoid valve. The stack is divided into two parts allowing a circulation of the hydrogen gas in the whole anode compartment between the two half-stacks. AFF stack is as efficient as the current hydrogen recirculation reducing the complexity and volume of the fuel cell systems. Benefits have been demonstrated on the weight of the anodic line (25% compared to pulsed ejector, and 43% compared to blower architecture) and on the costs (6% compared to pulsed ejector, and 57% compared to blower architecture).

For vehicle application, the sudden changes in current induce the most important degradations [22,50]. Water management is a key factor in fuel cell operation and it is accepted that a good hydration of the membrane facilitates proton conductivity and therefore is mandatory to obtain good performance. The management of this hydration depends both on the chosen fluidic architecture and the operating conditions of the system. An inefficient water management leads to flooding or drying out phenomena, which has a direct impact on fuel cell performance and lifespan. The drying out can induce local degradation within MEAs, particularly on the

membrane [26]. Paradoxically, a cell supplied with dry gas can be flooded [20,51]. The power profiles, for example, induce temperature and humidity cycles that can severely damage the stack, either at the membrane or at the electrode level [19,52,53]. Low current density operation has a tendency to flood the fuel cell due to a reduced flow rate and therefore poor fuel cell capacity to evacuate the water accompanied by a drop in temperature that accentuates the phenomenon. Several models for the formation of a water film on the catalytic layer have been developed to elucidate this phenomenon that occurs at low power [54,55].

As both modes of hydrogen feeding, the recirculation mode or the alternating fuel feeding one, exhibit similar performance results [48], this study focuses on a correlation between the anode architecture and fuel cell durability. One ageing test is performed for both hydrogen-feeding architectures considering test representative operating conditions and load cycles. The experimental data are analyzed at different scales up to the post-mortem expertise of membrane-electrode assemblies.

2. Material and methods

2.1. Fuel Cell system architecture

In order to compare the Alternating Fuel Feeding operation to the hydrogen recirculation, two different test benches are used. The first one is an autonomous 5-kW system already presented in previous studies [49,56]. The test bench has a classical configuration at the cathode, with an air filter, an air compressor and a passive membrane humidifier with flow through architecture. All the cells of the stack are connected in parallel to the cathodic line, and are equally fed with air. At the anode side, an AFF architecture is set up. With this new configuration, the stack is divided in two groups of cells. In this experiment, each group is located on one side of a central distribution plate. Hydrogen is supplied in one or the other half-stack, by means of two independent solenoid valves, labelled 1 and 2 on Figure S1.

In AFF operation, hydrogen is alternately supplied to each half-stack [49]. To do so, the solenoid valves 1 and 2 open alternately. When valve 1 is opened, the half-stack on the right side is fed with hydrogen from the outlet of the other half-stack (Figure S1-a). Conversely, when valve 2 is opened, the half-stack on the left side is fed by hydrogen from the outlet of the half-stack on the right side (Figure S1-b). Finally, the hydrogen outlet being closed by valve 3 during the alternating hydrogen supply, liquid water is collected in the central distribution plate, and nitrogen concentration increases in the anodic gas mixture. Both species are evacuated periodically when valve 3 is opened together with valves 1 and 2, as represented on Figure S1-c. The complete sequence of AFF operation is provided in Rodosik et al. [49].

The second test bench is a commercial Greenlight G100 fuel cell bench that can test fuel cell stacks of a few hundred watts. The flow rate, pressure, temperature and relative humidity are controlled on each line. This test bench is used in order to simulate an operation in hydrogen recirculation. To do so, in the absence of a recirculating device, a gas mixture composed of hydrogen and water vapor is injected at the inlet of the cell with a hydrogen stoichiometric ratio of 1.5, which is frequently used with this stack technology [24]. Hydrogen stoichiometric ratio is often set in the range 1.5-2.0, especially for high power operating points [35,57]. Greater stoichiometric ratios, like in the Toyota Mirai system [39], would not be suitable here, due to the large thickness of our membranes (25 μm). Indeed, high stoichiometric ratios associated with thin membranes allow adequate humidification of the MEAs without cathode humidifier, but it can have a detrimental effect on the stack performance if the membranes are too thick [58].

The anode relative humidity is set to 50%, regarding the stoichiometric ratio. Indeed, we can evaluate the relative humidity at the stack inlet from the mass balance of a recirculation loop. If we consider that the exit valve of the loop is closed, and if we assume that the gas is saturated with water vapor at the stack outlet, the gas relative humidity RH at the stack inlet is linked to the stoichiometric ratio SR through the equation:

$$RH = \frac{1}{\frac{P_{sat}}{P} + \frac{SR}{SR-1} \left(1 - \frac{P_{sat}}{P}\right)} \quad (1)$$

Where P is the total pressure and P_{sat} the saturation pressure for water vapor, both assumed constant in the hydrogen loop. With this simplified approach, a total pressure of 1.3 bar and a temperature of 80°C leads to a relative humidity of 45%. Thus, imposing a value of 50% during the test that simulates the operation with a recirculation loop is a valid approximation.

The presence of nitrogen in the actual mixture is neglected. The stack tested on this test bench will be called “Recirculation stack”.

The stack tested in AFF operation is composed of two half-stacks of 35 cells on each side of a central plate, leading to 70 cells. For the test of the recirculation operation, another stack of the same technology (same bipolar plates and MEAs) is assembled with one group of eight cells, and no central plate. Its configuration in terms of fluidic feeds is classical. All the manifolds connect the cells in parallel, either for injection or evacuation of the fluids. Membrane Electrode Assemblies with active area 220 cm^2 are assembled with serpentine design bipolar plates. Even though the fluid distribution in the cells is not performed with parallel channels, it can be considered that air and hydrogen circulate in counter-flow during the recirculation operation, regarding the positions of the inlets and outlets (indicated on Figure S3 and on Figure 5), and the configuration of the serpentine channels. In AFF operation, the gas

circulation alternates co-flow and counter-flow modes. More details about the design of bipolar plates and MEAs are given in previous work [59,60].

2.2. Test Protocol

Similar ageing tests are performed in this study for the two hydrogen feeding architectures. The test is based on the Fuel Cell Dynamic Load Cycle (FC-DLC) [61], and similar operating conditions are applied to both stacks, except for hydrogen feeding. The duration of both tests is approximately 1000 hours.

The reference FC-DLC load cycle is simplified due to power limitations of the test bench, keeping a few different current density steps as illustrated in Figure S2. This adaptation of the cycle consists in a squaring of the current density pulses. As a consequence, some losses of accuracy are observed by comparison to the genuine dynamic load profile. However, the current density of 0.42 A cm^{-2} still represents approximately 50 % of the maximum current density achievable with this stack technology. In contrast, typical driving cycles tested with the Toyota Mirai by Argonne National Laboratory induce a low power demand. Thus, the maximum power provided by the Mirai stack to cover 90 % of the NEDC power demand is only 10% of its maximum power [62]. Even without high power peaks, the simplified FC-DLC cycle defined here remains dynamic and harsh.

The operating conditions for both tests are chosen according to automotive conditions. All parameters are gathered in Table 1. The temperature is maintained at a high level of 80°C . The relative humidity at the cathode is quite low, due to the consideration of a volume constraint for the system, leading to a downsizing of the passive humidifier. The relative humidity is set to around 30% at the cathode side on both test benches with AFF and passive humidification.

Alternating Fuel Feeding introduces some specific operating parameters, such as the AFF frequency. The latter corresponds to the switching frequency of the two inlet valves (1 and 2). The sensitivity analysis presented previously [49] about the operating parameters that are specific to AFF shows that an AFF frequency of 0.7 Hz is optimal in this case. Furthermore, the outlet valve 3 is opened regularly during one second in order to purge the anode circuit. A purge period of 70 seconds is selected. The amount of hydrogen rejected during the purges is equivalent to 2% of the hydrogen consumption inside to stack, leading to an average stoichiometric ratio of 1.02 at the anode.

Table 1: Experimental parameters for ageing tests

Anodic architecture	AFF (0.7Hz)	Recirculation
Cell number	70	8
Relative humidity anode/cathode (%)	-/30 ± 2	50/30
Stack stoichiometry H₂/air	1.02/1.8	1.5/1.8
Outlet temperature of the stack	80°C	80°C
Inlet gas pressure	1.3 bar	1.3 bar

2.3. Characterization methods

PEMFC degradations are characterized at the stack scale as well as at the cell one. At the stack scale, operating heterogeneities between cells may appear, while, at the cell scale, local operating heterogeneities on the surface of the MEAs can be detected.

2.3.1. In-situ diagnosis

The distribution of the current density and temperature over the cell area is measured using a Current Scan Lin S++ [63] device apparatus. This local in-situ diagnosis is a custom-built segmented printed circuit board inserted between two cells inside the stack. Local current is measured using ring cores of a magnetically soft material (ferrite). The size of the segments is approximately 7 x 7 mm. Therefore, for a 220 cm² active area, the current distribution is measured by using 480 measuring segments. The board is also equipped with 120 temperature sensors, based upon the dependency of the resistivity of metals such as copper upon temperature. The current density is measured with a precision of 0.02 A cm⁻², and the temperature with a precision of 1 °C. This sensor plate, placed inside the stack between two bipolar plates, replaces one membrane electrode assembly. The gas channels in contact with the sensor plate are not fed with reactants.

In addition to the current density distribution measurement, a set of analysis is performed throughout the ageing test [24]. Punctual polarization curves are performed each 200 h. Moreover, Linear Sweep Voltammetry (LSV) and Cyclic Voltammetry (CV) are also performed for both stacks in order to characterize respectively the evolution of the hydrogen permeation through the membrane and the electrochemical active surface area (ECSA) loss at the cathode. During the electrochemical characterization test (CV), nitrogen flows over the working electrode while hydrogen flows over the counter-electrode. For the CV curves measurement, the cathode potential ranges from 0.05V to 0.80V vs. standard hydrogen electrode with a scan rate of 50 mV s⁻¹. The ECSA are estimated based on the calculation of the area of the

desorption/adsorption peak of a monolayer of hydrogen adsorbed on the Pt catalyst surface and after subtracting the contribution of the double layer charge. Permeation measurement (Linear Sweep voltammetry) consists in applying a potential ramp to an electrochemical cell with a scanning rate close to 1 mV/s. The voltage applied to a single cell ranges from 0.05 V to a maximum of 0.7 V. The resulting current is measured and correspond to the quantity of hydrogen crossing the membrane. The stack in recirculation is characterized each 200 h while the one in AFF only each 500h for technical reason.

All cells in the Recirculation stack are monitored. This is not the case in AFF mode due to the size of the stack. The location of the tested cells is chosen either because of their singular position (extreme cells) in the stack, or because of their particular behavior. The LSV is used to study the evolution of the hydrogen permeation through the membrane for all the cells of the Recirculation stack and only for eight cells on the AFF stack.

2.3.2. Post-mortem analyses of the PEMFC stack

At the end of life, postmortem analyses are performed in order to investigate the MEA degradation using different characterization methods.

Potential cracks or pinholes in the aged MEA can be, first, located by using a hydrogen box associated to an infrared camera. In this device, diluted hydrogen flows in the box, on the back side of the aged MEA, while atmospheric air is present at the front-side of the MEA, namely outside of the box. Eventual pinholes or cracks in the membrane can be detected by hot spots. Indeed, they form direct paths between both sides of the MEA, and induce a direct combustion of hydrogen in air. Images of the whole active area of a MEA obtained with an infrared camera (FLIR® E-Series Advanced Thermal Imaging Camera) provide mappings of the permeation rate of hydrogen through the membrane. High permeation rates are detected where the temperature is high and are associated with pinholes or cracks. This post-mortem analysis technique has already been used and described in previous studies [24].

Moreover, mini-cell tests are performed in order to evaluate the local behavior of the MEAs after the tests. These cells have an active area of less than 2 cm², and are dedicated to the characterization of the electrochemical performance of catalytic layers and gas diffusion layers. The effect of mass transports in the channels is neglected due to the use of high reactant flows, corresponding to stoichiometric ratios greater than 10 [64]. Therefore, 1.8 cm² rectangular samples are cut in several aged MEA in different locations, such as near the gases inlets, in the cell center and near the gases outlets. Once inserted in the mini-cell device, their ECSA are measured using the Cyclic Voltammetry. The selection and location of the areas to be cut are made using current and temperature density maps (Figure S3). In total, six zones are cut

out, in Air Inlet (AI), Air Outlet (AO), Hydrogen Inlet (HI), Hydrogen Outlet (HO) and in the middle of a Hot Spot (HS) supposedly drier, and of a Cold Spot (CS) supposedly wetter.

Different operating conditions are tested on each sample. These are grouped in Table 2. Each sample is first subjected to the so-called favorable conditions and then the sensitivity to moisture is analyzed by comparing behavior in dry and wet conditions.

Table 2: Operating conditions tested on differential cells

Condition	Polarization curve			ECSA measurement
	Favorable	Dry	Wet	Ambient
Temperature (°C)	80	80	60	25
Pressure (bar)	1.5			1.5
Relative Humidity (%) anode/cathode	80/80	50/50	80/80	100
Gas	H ₂ /Air			H ₂ /N ₂

Finally, samples from a reference MEA and from the six zones of several aged MEAs are analyzed by Scanning Electron Microscopy (SEM), and compared.

3. Experimental results

3.1. *In situ analysis*

3.1.1. Stack scale

The following section presents an analysis at the stack scale for a global understanding of degradation phenomena.

The global performances of the two stacks are recorded on a characterization bench at the beginning and end of the test under system conditions of 80°C, 1.3 bar, with stoichiometric ratios (SR) at the anode and the cathode of respectively 1.5 and 1.8 and relative humidity (RH) of respectively 50% and 30%. The polarization curves at the beginning and end of the test are shown in Figure 1. The general pattern of the curves between the beginning and end of the test shows similar performance.

At the beginning of the test, the two polarization curves of the 8-cell recirculating stack and of the 70-cell AFF stack are superimposed. A slight deviation can be observed at high current densities ($> 0.5 \text{ A.cm}^{-2}$) where a mass transport effect begins to build up on the AFF stack. This difference might be due to the endplates design of the AFF stack, which are not optimized for flow-through mode used in the characterization process or to the test facilities, which have

quite different power ranges. However, in the target operating range (cycle < 0.42 A cm⁻²), the performances obtained in both cases are comparable. This result confirms that the MEA batches are similar, and that the stack configuration and size have no impact on the initial performance if current density is lower than 0.5 A/cm².

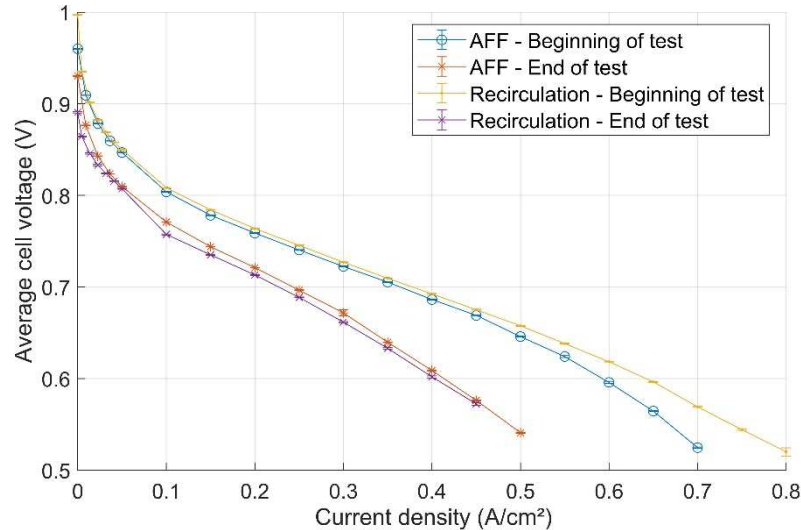


Figure 1: Polarization curves of the two stacks tested in durability at the beginning and end of the test (80°C, 1.3 bar, SR=1.5/1.8, RH 50/30%).

At the end of the test, again the polarization curves of both stacks are superimposed. The decrease in overall performance is almost the same for both configurations. At a current density of 0.42 A cm⁻², the drop in performance reaches 90 mV in recirculation and 89 mV in AFF. However, the voltage drop in open circuit is greater in recirculation than in AFF. This voltage is less than 900 mV at the end of the test in recirculation, whereas it reaches 930 mV on the AFF stack.

At the beginning of life, the maximum standard deviation between the cell voltages is less than 8 mV in recirculation, and less than 14 mV in AFF. At the end of life, the maximum standard deviation between cell voltages is higher and is about 50 mV for the recirculation test and only 22 mV for AFF.

Degradation rates are calculated for each cell and for different current levels, namely 0.1 and 0.42 A cm⁻² obtained from the adapted FC-DLC speed cycle. They correspond to the slope of the linear regression plotted for all cell voltage measurements collected during the test at the same current. By comparing degradation rates of individual cells, heterogeneities in behavior between cells within the same stack can be observed.

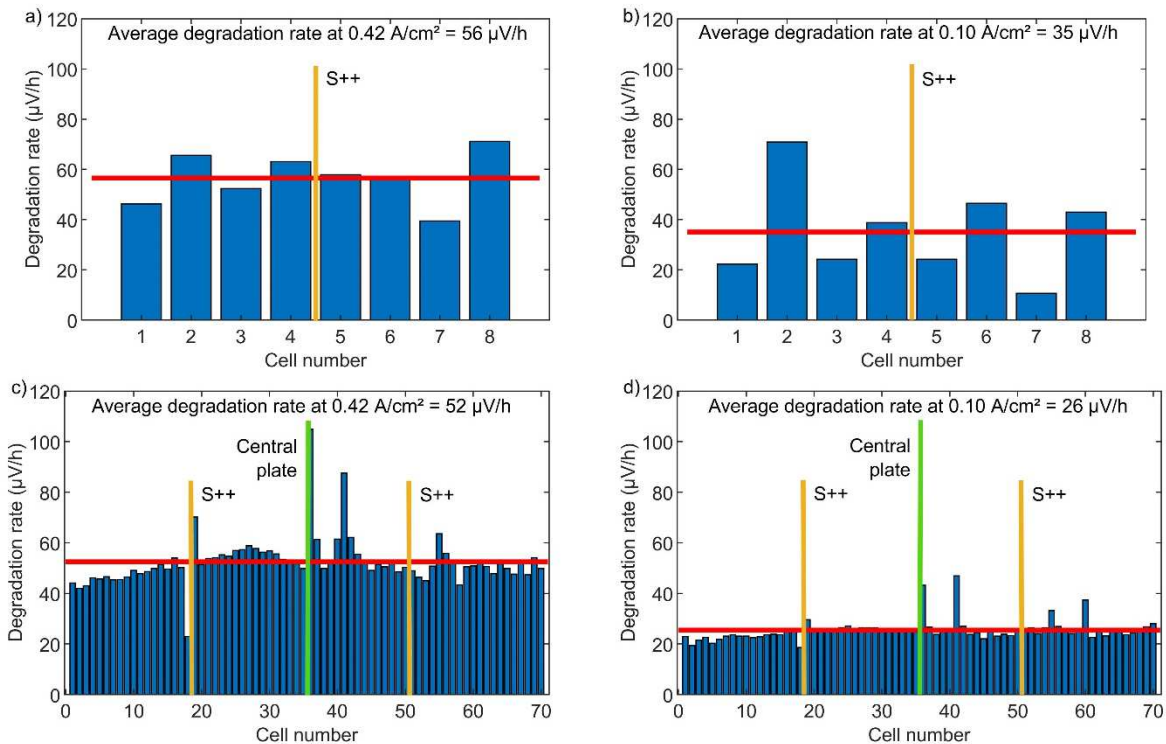


Figure 2: Degradation rates of individual cell in both stacks and location of the S++® measurement board a) at 0.42 A cm⁻² with recirculation, b) at 0.1 A cm⁻² with recirculation, c) at 0.42 A cm⁻² with AFF and d) at 0.1 A cm⁻² with AFF.

Figure 2 shows the degradation rates for each cell in both stacks at 0.42 A cm⁻² and 0.1 A cm⁻². The values for the stack aged in recirculation are represented on Figure 2-a and 2-b. At the higher current density (0.42 A cm⁻²) on the plateau of the load cycle, the average degradation rate is 56 µV/h. This value is high but consistent with degradation rates obtained with this stack design in other tests [24]. At lower current density (0.1 A cm⁻²), the heterogeneity of the degradation rates increase, with a standard deviation of 19 µV/h, and two groups of cells can be distinguished. Four of these, namely cells 2, 4, 6, and 8, have rates well above the calculated average of 35 µV/h. For instance, cell 2 even reaches a maximum of 70 µV/hour.

Figure 2-c and 2-d show the degradation rates obtained for the aged AFF stack at the same current densities as the recirculating stack. Figure 2-a shows the degradation rates for a current density of 0.42 A cm⁻² while Figure 2-b corresponds to 0.1 A cm⁻². The S++® measurement boards are located in the middle of the stacks. The average degradation rate is 52 µV/h, which is almost similar to that measured in recirculation at the same current density.

The cells seem to degrade homogeneously except a few ones: 18, 19, 36, 41 and 55. Cells 18 and 19 may be affected by the presence of the S++® measurement device. Cell 36, in contact with the central distribution plate, has a special location from the stack design point of view. The latter is generally colder than the other ones and seems to be flooded more easily,

especially at the anode. This may explain its very high degradation rate. Avoiding this particular issue in future stacks is crucial. It might require an improvement of the flow fields inside the cell and the stack, and a better thermal management of the stack.

At low current (0.1 A cm^{-2}), a few cells exhibit degradation rates well above the average of $25 \mu\text{V/h}$. Cells with high degradation rates at low current also have high degradation rates at high current. Only cell 60 seems to be degraded at low current but presents a degradation rate in the average at high current.

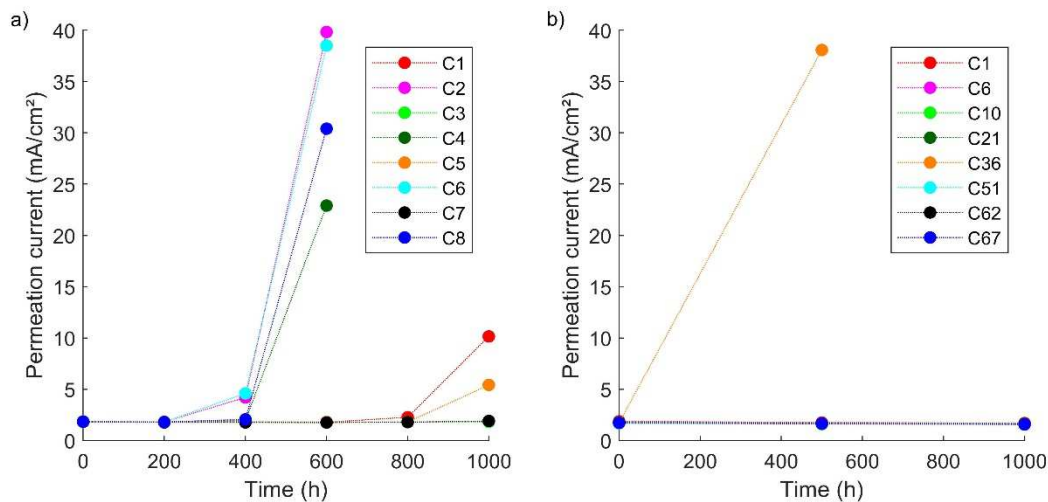


Figure 3: Permeation current for stacks aged in (a) recirculation mode and (b) AFF mode.

All the cells of the stack tested in recirculation mode undergo permeation current measurements every 200 hours during the durability test (Figure 3).

Among the cells of the stack in recirculation, four cells already identified in the previous section (cells 2, 4, 6 and 8) with a very low end-of-life OCV and high degradation rates show an early increase of their permeation current. It exceeds widely the nominal value of 1.8 mA cm^{-2} at 600 h of operation, and the following measurement points are out of range. Conversely, the permeation of the cells aged in AFF operation remains small even after 1000 hours of operation. Only the cell 36 located close to the central distribution plate exhibits a high permeation current after 500 hours of operation.

3.1.2. Cell scale

Current density distributions are measured in both stacks during ageing and at the beginning and end of the test. Figure 4 presents for both stacks the current density mappings at the beginning of the test, and the differential current density mappings between the beginning and the end of the test. The current density distributions represented on Figure 4-a and 4-b are

quite similar. A low current density region is observed at the air inlet, which may be due to a drying effect induced by the automotive conditions.

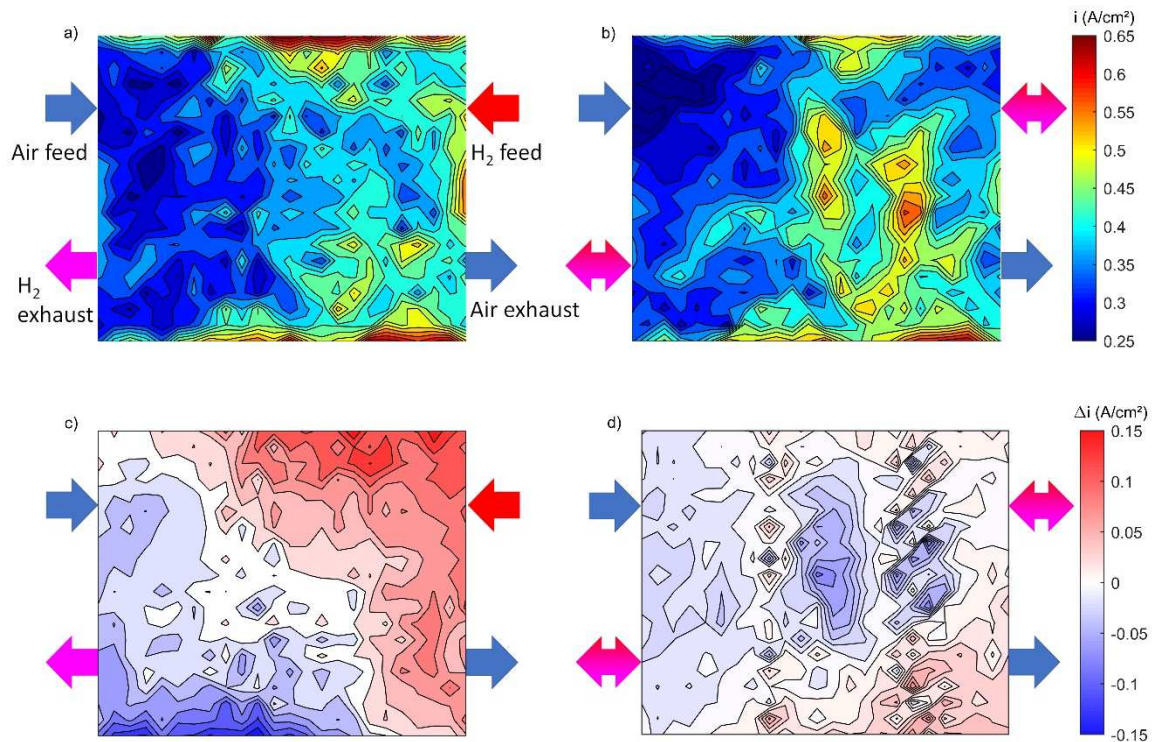


Figure 4: Current density distributions at the beginning of the test for (a) the stack in recirculation and (b) the AFF stack at 0.42 A cm⁻² and conditions detailed in Table 1; differential current density mappings in the same conditions calculated between the beginning and the end of the test (c) in recirculation and (d) in AFF

The differential current density mappings represented on Figure 4-c and 4-d are calculated between the end and the beginning of the test for the two stacks tested. They are calculated for the maximum current density of the cycle, i.e. 0.42 A cm⁻² and under the conditions of the durability test. The methodology consists in subtracting two current density distributions to obtain an image of the current density variation during a defined period. On the resulting mappings, the values are negative where the current density decreases over time.

The differential mapping obtained in recirculation mode has a less homogeneous distribution than in AFF. The evolution of the current densities shows a maximum decrease of 0.13 A cm⁻² during the test near the hydrogen outlet and an increase of 0.17 A cm⁻² close to the hydrogen inlet. This evolution is less noticeable in AFF with a maximum decrease of 0.12 A cm⁻² on the central hot spot and an increase of 0.09 A cm⁻² at the air outlet. This method shows that both stacks behave differently, because the differential mappings highlight distinct redistributions of the current with ageing.

3.2. Post-mortem ex-situ analysis

3.2.1. Permeation by infrared measurement

Permeation tests are performed with infrared measurements to identify pinholes or cracks formation on membranes. All the cells of the stack aged in recirculation and the majority of the cells aged in AFF mode are tested by infrared thermography. The results are summarized in Figure 5.

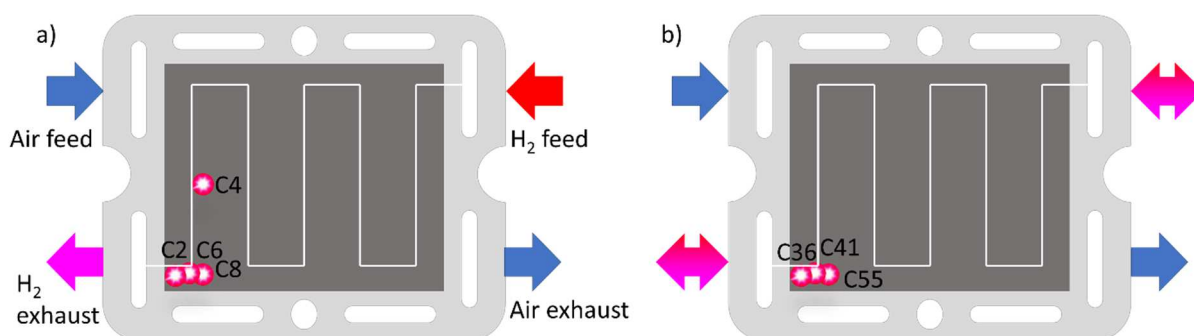


Figure 5: Location of the pinholes or cracks in the MEAs carried out with the infrared camera on (a) the recirculating aged stack and (b) the aged stack in AFF

Figure 5-a shows that four MEAs among the eight of the recirculating aged stack are drilled, while Figure 5-b highlights that only three drilled cells among the 70 aged in AFF mode. The pinholes are located close to the hydrogen outlet manifold in all cases. In recirculation, the pinholes in cells 2, 6 and 8 are very close to the hydrogen outlet manifold, while the pinhole in cell 4 is in the center of the last hydrogen channel.

3.2.2. Local measurement

Electroactive surface area and polarization curves in different conditions are measured for each mini-cell. Figure 6 shows polarization curves of samples from MEAs extracted from the stack in AFF mode in two different regions: Hydrogen Outlet (HO) and the central Hot Spot (HS) (see Figure S3).

Polarization curves are recorded in dry and wet conditions for the Hydrogen Outlet (HO) as well as the Hot Spot (HS). The performances of the two latter zones drop in wet condition at high current density, probably due to water flooding. Nevertheless, this phenomenon is observed only for a few cells of the AFF stack, and is never recorded for the stack in recirculation.

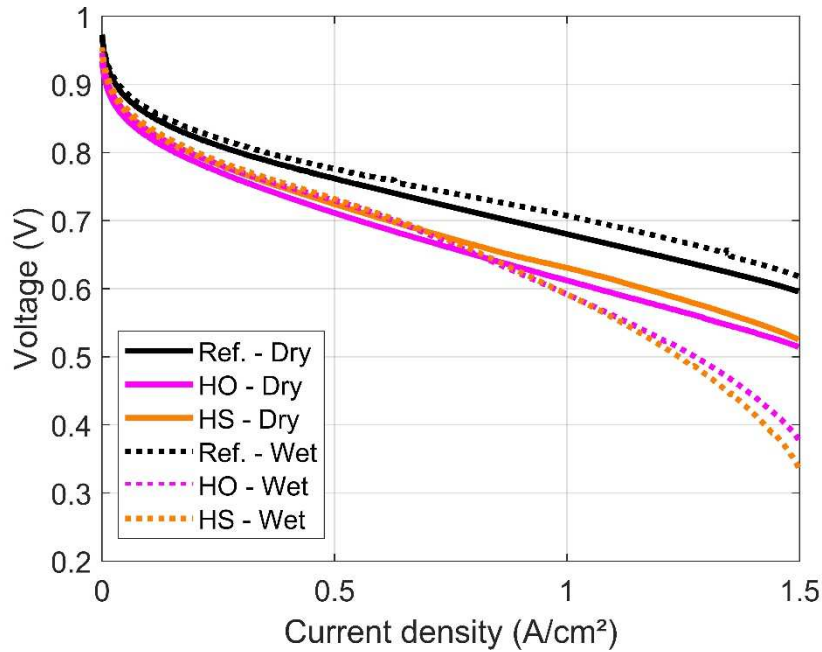


Figure 6: Local polarization curve recorded in dry and wet conditions (Stack in AFF)

Loss of active surface area is measured on several cells for the stacks in recirculation as well as in AFF. Whatever the case, the drop is lower than 10% of the initial value, which does not explain the observed performance loss. This observation is in accordance with previous analyses conducted with the same MEA technology [24,65].

To go further, Figure 7 shows the SEM images taken in the Air Inlet zone (AI). In recirculation, as shown in Figure 7-a, the area seems very degraded. A compaction of the cathode catalytic layer is observed. Its thickness has been reduced to 4 μm instead of the 13 μm initially measured. The zone is very clear, highlighting a high platinum concentration. The decrease in thickness is attributed to corrosion of the electrode carbon support, which modifies its microstructure by reducing its porosity. Figure 7-c and 7-d show SEM images obtained on the AFF stack at the Air Inlet zone (AI). The structure of the electrode does not appear to have changed compared to the reference sample. The thickness of the cathode at 14 μm is close to the reference. In the other locations on the MEAs (Air Outlet, Hot and Cold Spot, Hydrogen Inlet and Outlet), the cathodes are always thinner than initially with thicknesses around 11 μm in both recirculation and AFF modes.

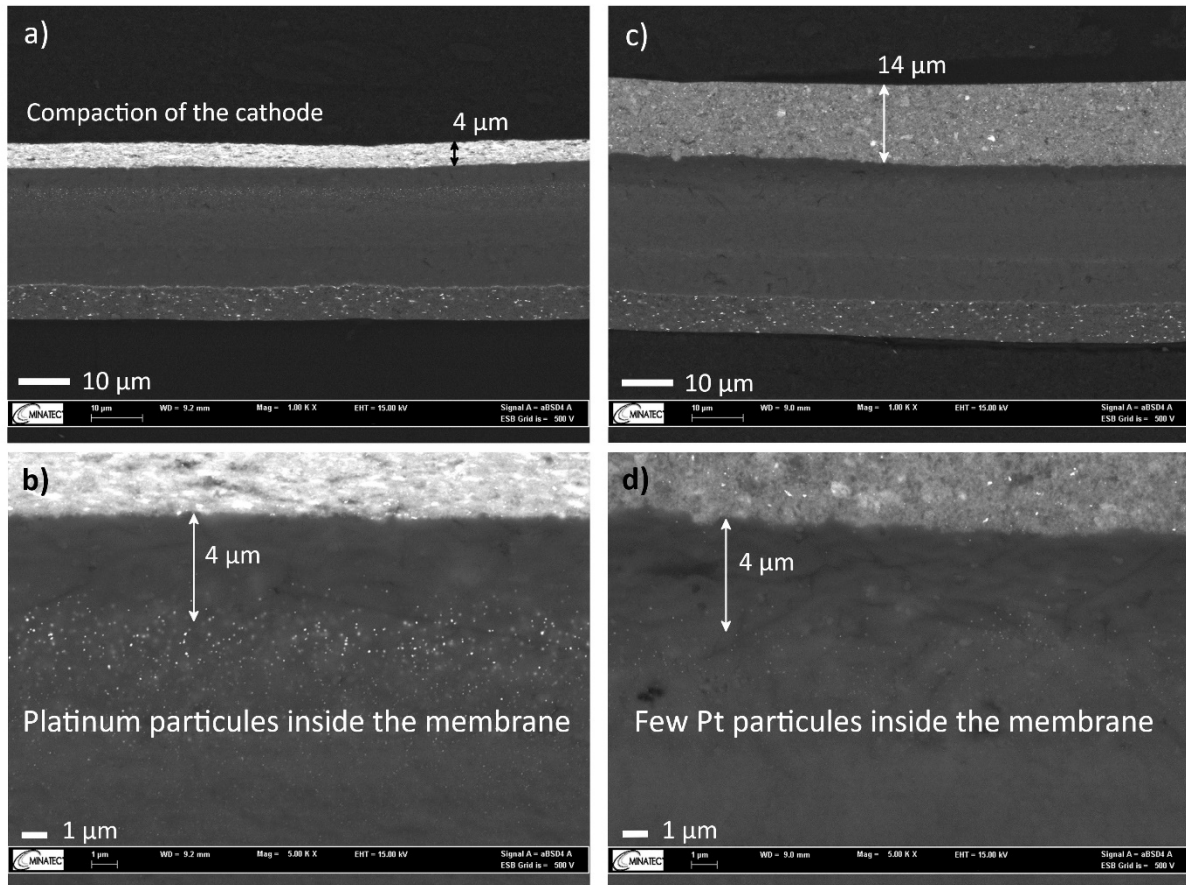


Figure 7: Cross-sectional SEM images of the air inlet area of an aged MEA and zoom on the membrane area near the cathode to visualize the precipitated Platinum deposition, a) and b) in recirculation, and c) and d) in AFF

Finally, a platinum band is clearly visible in the membrane at a few μm from the cathode indicating that a mechanism for dissolving and then precipitating the platinum in the membrane has taken place. This phenomenon occurs at Hydrogen outlet, Air Inlet (Figure 7-c) and Hot Spot (HO, AI, HS) in recirculation mode, while it occurs in AFF mode at Hydrogen Inlet/Outlet, Cold Spot and Air Outlet (HI, HO, CS, AO).

4. Discussion

The multi-scale analysis of the degradations in the two stacks, each subjected to a different operating mode, first shows similar behaviors. After a current cycling test of more than 1000h, the degradation rates calculated at 0.42 A cm^{-2} are equivalent: $56 \mu\text{V/h}$ in recirculation and $52 \mu\text{V/h}$ in AFF. However, there are local differences related to the anodic fluidic architectures.

In recirculation, the Hydrogen Outlet (HO) and Air Inlet (AI) are the most degraded areas. The performances recorded by the local current density measurement in this zone are the worst at the beginning of the test and they degrade with ageing. After the test, half of the MEAs in this

stack are drilled in these areas. In AFF, a performance decay is observed close to the Air Inlet (AI) and attributed to the drying out during operation. Nevertheless, the highest current density decrease is recorded in zones in the middle of the cell where MEA degradation is the strongest during ageing. The performance decay observed in the central region is likely due to the specific thermal management of the bipolar plates design. Frey et al. [24] well described the temperature distribution of this stack technology and its impact on water management as well as durability. A temperature hot spot is identified in the central area often leading to membrane drying and thus lower performance. The different current decrease distribution and degradation observed in the two tests indicates that each hydrogen feeding strategy leads to specific local degradations, while the global performance degradation is similar.

Figure 8 presents a summary of the observed local degradation for both operating modes. All identified degradations are superimposed on temperature distribution mapping obtained in the tested conditions at 0.42 A/cm^2 (like in Figure 4). It can be observed that the temperature difference between inlet and outlet is lower in recirculation than in AFF. This is due to the test facilities. The minimum cooling flow reached with test bench used for recirculation was slightly higher than the one reached on the system test bench. Therefore, cooling water temperature difference was lower in recirculation. A lower temperature difference would favor the durability with lower degradation rates. However, this was not observed during the test. During this test and in the target operation range, it seems that cooling temperature difference did not play a major role in degradation occurrence.

Among the observed degradations, membrane drilling, represented by red discs, is observed in both cases at the hydrogen outlet, but it is more frequent in recirculation than in AFF. Local cell flooding events are suspected to explain these degradations. They might be less frequent, or have less impact, in AFF compared to recirculation.

The decrease of the active area, represented by an orange disc, remains generally weak, except close to the hydrogen outlet in recirculation. It can be assumed that the membrane holes may have exacerbated these degradations in this zone. In AFF mode, this type of degradation is observed in a more moderate way in Hydrogen Outlet (HO) and in the Cold Spot (CS). The presence of liquid water in these areas could favor the loss of active surface.

Another difference observed between recirculation and AFF modes is the corrosion of the carbon support of the electrodes (orange squares), which can be also correlated to a decrease of the active area. This degradation mode is mainly associated with hydrogen starvation, which can occur locally where the anode is flooded with water, blocking the hydrogen access to the catalyst. This phenomenon is mainly observed, for the stack in recirculation, at the air inlet. A similar corrosion is recorded in the central hot zone of the stack but with a lower amplitude.

Conversely, carbon corrosion is not observed in AFF mode whatever the location on the electrode surface area.

Moreover, the distribution of water in the cell components is again questioned to explain the precipitation of Platinum in the membrane (symbolized by an orange triangle on Figure 8). This degradation phenomenon is generally related to important voltage variations, associated with wet conditions. In recirculation, the condensation of water at the anode outlet generates wetter conditions throughout the left half of the active surface, thus favoring the precipitation of platinum. In AFF, the wettest areas are the air outlet and the hydrogen inlet and outlet, as well as the cold environment where Platinum precipitation is observed in the membrane.

Finally, the last type of degradation relates to the loss of hydrophobicity of the electrodes (green squares). This is usually favored by a high temperature and strong variations in humidity. This is the case in AFF where the variations in relative humidity at the anode are very strong (from 0 to 100% RH at each purge cycle). The hypothesis of loss of hydrophobicity has not been validated by dedicated analyses. It will be the subject of a complementary study by measuring, for example, the contact angles of water on the GDL.

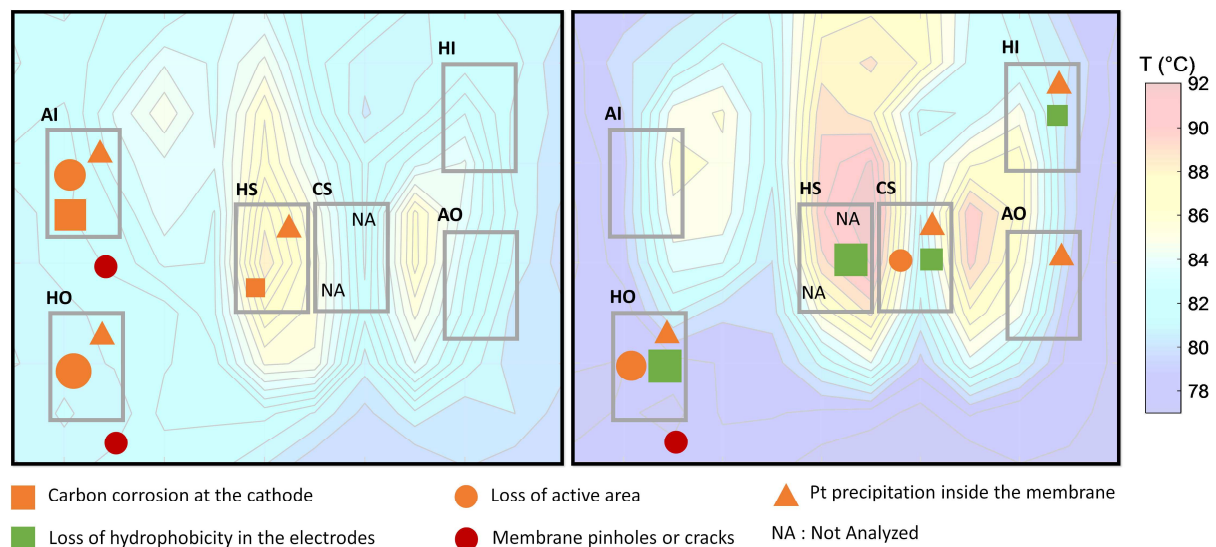


Figure 8: Graphical summary of the main degradations deduced from local post-mortem analyses schematized on temperature maps a) in recirculation and b) in AFF

5. Conclusion

The AFF architecture allows to simplify the system complexity and to reduce significantly the weight of the anodic line maintaining similar performance levels in comparison to recirculation one. In this work, one ageing test has been performed for a classical mode of recirculation of hydrogen and for the alternating fuel feeding one, implementing the Fuel Cell Dynamic Load Cycle (FC-DLC). Overall, the degradation rates of stack performances are quite similar in both

cases along with the ageing. Indeed, polarization curves highlighted only a slight deviation at OCV and at high currents densities.

At the cell scale, the hydrogen feeding mode induces heterogeneous ageing processes on the different components. Indeed, the most degraded areas are observed close to the hydrogen outlet and air inlet in recirculation mode while degraded areas are more uniformly distributed on the cell in AFF mode. Moreover, the degradation processes seem to be also different for both modes. On one hand, both architectures trigger the occurrence of membrane pinholes and micro-cracks at the hydrogen outlet responsible for a sudden loss of functionality of the cells. On the other hand, the recirculation hydrogen mode accelerates cathode catalyst layer corrosion close to the hydrogen outlet (HO) and air inlet (AI) while the AFF mode might favor loss of hydrophobicity of the electrodes in some areas.

This study highlights the fact that the hydrogen feeding strategy has a noticeable influence on the distribution of the local degradation along the cell, and on the current density distribution. For durability improvement purposes, the study of Bipolar Plate designs could help in optimizing the gas flows and temperature distribution.

Acknowledgements

The authors are grateful to the French Commissariat à l'Energie Atomique (CEA), which supported this work, and to F. Sauzedde, L. Rouillon, L. Jacqmin and S. Germe for their help during the realization of the test program.

References

- [1] Fuel Cell and Hydrogen Joint Undertaking. Addendum to the Multi - Annual Work Plan 2014 - 2020. 2018. <https://www.fch.europa.eu/page/multi-annual-work-plan> (accessed May 18, 2021).
- [2] Thompson ST, James BD, Huya-Kouadio JM, Houchins C, DeSantis DA, Ahluwalia R, et al. Direct hydrogen fuel cell electric vehicle cost analysis: System and high-volume manufacturing description, validation, and outlook. *Journal of Power Sources* 2018;399:304–13. <https://doi.org/10.1016/j.jpowsour.2018.07.100>.
- [3] US Department of Energy. DOE Technical Targets for Polymer Electrolyte Membrane Fuel Cell Components. EnergyGov 2016. <https://www.energy.gov/eere/fuelcells/doe-technical-targets-polymer-electrolyte-membrane-fuel-cell-components> (accessed March 24, 2020).
- [4] Abbou S, Dillet J, Spornjak D, Mukundan R, Fairweather JD, Borup RL, et al. Time Evolution of Local Potentials during PEM Fuel Cell Operation with Dead-Ended Anode. *ECS Trans* 2013;58:1631–42. <https://doi.org/10.1149/05801.1631ecst>.

- [5] Abbou S, Dillet J, Maranzana G, Didierjean S, Lottin O. Impact of Water Management on Local Potential Evolutions during PEM Fuel Cell Operation with Dead-Ended Anode. *ECS Trans* 2015;69:1267–76. <https://doi.org/10.1149/06917.1267ecst>.
- [6] Dubau L, Castanheira L, Chatenet M, Maillard F, Dillet J, Maranzana G, et al. Carbon corrosion induced by membrane failure: The weak link of PEMFC long-term performance. *International Journal of Hydrogen Energy* 2014;39:21902–14. <https://doi.org/10.1016/j.ijhydene.2014.07.099>.
- [7] Asghari S, Ashraf Khorasani MR, Dashti I. Investigation of self-humidified and dead-ended anode proton exchange membrane fuel cell performance using electrochemical impedance spectroscopy. *International Journal of Hydrogen Energy* 2016;41:12347–57. <https://doi.org/10.1016/j.ijhydene.2016.05.133>.
- [8] Siegel JB, McKay DA, Stefanopoulou AG, Hussey DS, Jacobson DL. Measurement of Liquid Water Accumulation in a PEMFC with Dead-Ended Anode. *J Electrochem Soc* 2008;155:B1168–78. <https://doi.org/10.1149/1.2976356>.
- [9] Lee Y, Kim B, Kim Y. An experimental study on water transport through the membrane of a PEFC operating in the dead-end mode. *International Journal of Hydrogen Energy* 2009;34:7768–79. <https://doi.org/10.1016/j.ijhydene.2009.07.010>.
- [10] Abbou S, Dillet J, Maranzana G, Didierjean S, Lottin O. Local potential evolutions during proton exchange membrane fuel cell operation with dead-ended anode – Part II: Aging mitigation strategies based on water management and nitrogen crossover. *Journal of Power Sources* 2017;340:419–27. <https://doi.org/10.1016/j.jpowsour.2016.10.045>.
- [11] Kocha SS, Yang JD, Yi JS. Characterization of gas crossover and its implications in PEM fuel cells. *AIChE Journal* 2006;52:1916–25. <https://doi.org/10.1002/aic.10780>.
- [12] Ahluwalia RK, Wang X. Buildup of nitrogen in direct hydrogen polymer-electrolyte fuel cell stacks. *Journal of Power Sources* 2007;171:63–71. <https://doi.org/10.1016/j.jpowsour.2007.01.032>.
- [13] Baik KD, Kim MS. Characterization of nitrogen gas crossover through the membrane in proton-exchange membrane fuel cells. *International Journal of Hydrogen Energy* 2011;36:732–9. <https://doi.org/10.1016/j.ijhydene.2010.09.046>.
- [14] Paganelli G. Fuel Cell and Method for Stopping a Fuel Cell. US20120308906A1, 2012.
- [15] Nikiforow K, Karimäki H, Keränen TM, Ihonen J. Optimization study of purge cycle in proton exchange membrane fuel cell system. *Journal of Power Sources* 2013;238:336–44. <https://doi.org/10.1016/j.jpowsour.2012.11.153>.
- [16] Meyer Q, Ashton S, Torija S, Gurney C, Boillat P, Cochet M, et al. Nitrogen Blanketing and Hydrogen Starvation in Dead-Ended-Anode Polymer Electrolyte Fuel Cells Revealed by Hydro-Electro-Thermal Analysis. *Electrochimica Acta* 2016;203:198–205. <https://doi.org/10.1016/j.electacta.2016.04.018>.

- [17] Abbou S, Dillet J, Maranzana G, Didierjean S, Lottin O. Local potential evolutions during proton exchange membrane fuel cell operation with dead-ended anode – Part I: Impact of water diffusion and nitrogen crossover. *Journal of Power Sources* 2017;340:337–46. <https://doi.org/10.1016/j.jpowsour.2016.11.079>.
- [18] Pozio A, Silva RF, De Francesco M, Giorgi L. Nafion degradation in PEFCs from end plate iron contamination. *Electrochimica Acta* 2003;48:1543–9. [https://doi.org/10.1016/S0013-4686\(03\)00026-4](https://doi.org/10.1016/S0013-4686(03)00026-4).
- [19] Lee H, Kim T, Sim W, Kim S, Ahn B, Lim T, et al. Pinhole formation in PEMFC membrane after electrochemical degradation and wet/dry cycling test. *Korean J Chem Eng* 2011;28:487–91. <https://doi.org/10.1007/s11814-010-0381-6>.
- [20] Sanchez DG, Garcia-Ybarra PL. PEMFC operation failure under severe dehydration. *International Journal of Hydrogen Energy* 2012;37:7279–88. <https://doi.org/10.1016/j.ijhydene.2011.11.059>.
- [21] Guétaz L, Escribano S, Sicardy O. Study by electron microscopy of proton exchange membrane fuel cell membrane-electrode assembly degradation mechanisms: Influence of local conditions. *Journal of Power Sources* 2012;212:169–78. <https://doi.org/10.1016/j.jpowsour.2012.03.096>.
- [22] Pei P, Chen H. Main factors affecting the lifetime of Proton Exchange Membrane fuel cells in vehicle applications: A review. *Applied Energy* 2014;125:60–75. <https://doi.org/10.1016/j.apenergy.2014.03.048>.
- [23] Qiu Y, Zhong H, Wang M, Zhang H. Effect of relative humidity cycles accompanied by intermittent start/stop switches on performance degradation of membrane electrode assembly components in proton exchange membrane fuel cells. *Journal of Power Sources* 2015;283:171–80. <https://doi.org/10.1016/j.jpowsour.2015.02.134>.
- [24] Nandjou F, Poirot-Crouvezier J-P, Chandesris M, Blachot J-F, Bonnaud C, Bultel Y. Impact of heat and water management on proton exchange membrane fuel cells degradation in automotive application. *Journal of Power Sources* 2016;326:182–92. <https://doi.org/10.1016/j.jpowsour.2016.07.004>.
- [25] Zhao J, Shahgaldi S, Li X, Liu Z (Simon). Experimental Observations of Microstructure Changes in the Catalyst Layers of Proton Exchange Membrane Fuel Cells under Wet-Dry Cycles. *J Electrochem Soc* 2018;165:F3337–45. <https://doi.org/10.1149/2.0391806jes>.
- [26] Sanchez DG, Ruiu T, Biswas I, Schulze M, Helmly S, Friedrich KA. Local impact of humidification on degradation in polymer electrolyte fuel cells. *Journal of Power Sources* 2017;352:42–55. <https://doi.org/10.1016/j.jpowsour.2017.03.057>.

- [27] Rabbani A, Rokni M. Effect of nitrogen crossover on purging strategy in PEM fuel cell systems. *Applied Energy* 2013;111:1061–70. <https://doi.org/10.1016/j.apenergy.2013.06.057>.
- [28] Chen J, Siegel JB, Stefanopoulou AG, Waldecker JR. Optimization of purge cycle for dead-ended anode fuel cell operation. *International Journal of Hydrogen Energy* 2013;38:5092–105. <https://doi.org/10.1016/j.ijhydene.2013.02.022>.
- [29] Han I-S, Jeong J, Shin HK. PEM fuel-cell stack design for improved fuel utilization. *International Journal of Hydrogen Energy* 2013;38:11996–2006. <https://doi.org/10.1016/j.ijhydene.2013.06.136>.
- [30] Strahl S, Husar A, Riera J. Experimental study of hydrogen purge effects on performance and efficiency of an open-cathode Proton Exchange Membrane fuel cell system. *Journal of Power Sources* 2014;248:474–82. <https://doi.org/10.1016/j.jpowsour.2013.09.122>.
- [31] Sasmito AP, Ali MI, Shamim T. A Factorial Study to Investigate the Purging Effect on the Performance of a Dead-End Anode PEM Fuel Cell Stack. *Fuel Cells* 2015;15:160–9. <https://doi.org/10.1002/fuce.201300069>.
- [32] Werner C, Busemeyer L, Kallo J. The impact of operating parameters and system architecture on the water management of a multifunctional PEMFC system. *International Journal of Hydrogen Energy* 2015;40:11595–603. <https://doi.org/10.1016/j.ijhydene.2015.02.012>.
- [33] Eskin MG, Yeşilyurt S. Anode bleeding experiments to improve the performance and durability of proton exchange membrane fuel cells. *International Journal of Hydrogen Energy* 2019. <https://doi.org/10.1016/j.ijhydene.2019.02.152>.
- [34] Arboleda J. New Hyundai NEXO FCV, European Hydrogen Energy Conference, Malaga - Spain 2018.
- [35] Nikiforow K, Koski P, Ihonen J. Discrete ejector control solution design, characterization, and verification in a 5 kW PEMFC system. *International Journal of Hydrogen Energy* 2017;42:16760–72. <https://doi.org/10.1016/j.ijhydene.2017.05.151>.
- [36] Milewski J, Miller A, Sałaciński J. Off-design analysis of SOFC hybrid system. *International Journal of Hydrogen Energy* 2007;32:687–98. <https://doi.org/10.1016/j.ijhydene.2006.08.007>.
- [37] Marsano F, Magistri L, Massardo AF. Ejector performance influence on a solid oxide fuel cell anodic recirculation system. *Journal of Power Sources* 2004;129:216–28. <https://doi.org/10.1016/j.jpowsour.2003.11.034>.
- [38] Konno N, Mizuno S, Nakaji H, Ishikawa Y. Development of Compact and High-Performance Fuel Cell Stack. *SAE Int J Alt Power* 2015;4:123–9. <https://doi.org/10.4271/2015-01-1175>.

- [39] Hasegawa T, Imanishi H, Nada M, Ikogi Y. Development of the Fuel Cell System in the Mirai FCV, 2016, p. 2016-01–1185. <https://doi.org/10.4271/2016-01-1185>.
- [40] Zhao X, Xu L, Fang C, Jiang H, Li J, Ouyang M. Study on voltage clamping and self-humidification effects of pem fuel cell system with dual recirculation based on orthogonal test method. *International Journal of Hydrogen Energy* 2018;43:16268–78. <https://doi.org/10.1016/j.ijhydene.2018.06.172>.
- [41] Toghyani S, Afshari E, Baniasadi E. A parametric comparison of three fuel recirculation system in the closed loop fuel supply system of PEM fuel cell. *International Journal of Hydrogen Energy* 2019;44:7518–30. <https://doi.org/10.1016/j.ijhydene.2019.01.260>.
- [42] Uno M, Shimada T, Tanaka K. Reactant recirculation system utilizing pressure swing for proton exchange membrane fuel cell. *Journal of Power Sources* 2011;196:2558–66. <https://doi.org/10.1016/j.jpowsour.2010.10.094>.
- [43] Migliardini F, Capasso C, Corbo P. Optimization of hydrogen feeding procedure in PEM fuel cell systems for transportation. *International Journal of Hydrogen Energy* 2014;39:21746–52. <https://doi.org/10.1016/j.ijhydene.2014.08.070>.
- [44] Migliardini F, Di Palma TM, Gaele MF, Corbo P. Hydrogen purge and reactant feeding strategies in self-humidified PEM fuel cell systems. *International Journal of Hydrogen Energy* 2017;42:1758–65. <https://doi.org/10.1016/j.ijhydene.2016.06.196>.
- [45] Jiang H, Xu L, Fang C, Zhao X, Hu Z, Li J, et al. Experimental study on dual recirculation of polymer electrolyte membrane fuel cell. *International Journal of Hydrogen Energy* n.d. <https://doi.org/10.1016/j.ijhydene.2017.04.183>.
- [46] Lee H-Y, Su H-C, Chen Y-S. A gas management strategy for anode recirculation in a proton exchange membrane fuel cell. *International Journal of Hydrogen Energy* 2018;43:3803–8. <https://doi.org/10.1016/j.ijhydene.2018.01.026>.
- [47] Steinberger M, Geiling J, Oechsner R, Frey L. Anode recirculation and purge strategies for PEM fuel cell operation with diluted hydrogen feed gas. *Applied Energy* 2018;232:572–82. <https://doi.org/10.1016/j.apenergy.2018.10.004>.
- [48] De Grisard B, Achard P, Metkemeijer R. Long Term Performance of the Pressure Swing Recirculation System, IDHEA 2014 - International Discussion on Hydrogen Energy and Applications, Nantes, France 2014.
- [49] Rodosik S, Poirot-Crouvezier J-P, Bultel Y. Simplified anode architecture for PEMFC systems based on alternative fuel feeding: Experimental characterization and optimization for automotive applications. *International Journal of Hydrogen Energy* 2020;45:19720–32. <https://doi.org/10.1016/j.ijhydene.2020.05.014>.
- [50] Pei P, Chang Q, Tang T. A quick evaluating method for automotive fuel cell lifetime. *International Journal of Hydrogen Energy* 2008;33:3829–36. <https://doi.org/10.1016/j.ijhydene.2008.04.048>.

- [51] Gößling S, Klages M, Haußmann J, Beckhaus P, Messerschmidt M, Arlt T, et al. Analysis of liquid water formation in polymer electrolyte membrane (PEM) fuel cell flow fields with a dry cathode supply. *Journal of Power Sources* 2016;306:658–65. <https://doi.org/10.1016/j.jpowsour.2015.12.060>.
- [52] García-Salaberri PA, Sánchez DG, Boillat P, Vera M, Friedrich KA. Hydration and dehydration cycles in polymer electrolyte fuel cells operated with wet anode and dry cathode feed: A neutron imaging and modeling study. *Journal of Power Sources* 2017;359:634–55. <https://doi.org/10.1016/j.jpowsour.2017.03.155>.
- [53] O’Dea JR, Economou NJ, Buratto SK. Surface Morphology of Nafion at Hydrated and Dehydrated Conditions. *Macromolecules* 2013;46:2267–74. <https://doi.org/10.1021/ma302399e>.
- [54] Koz M, Kandlikar SG. Oxygen transport resistance at gas diffusion layer – Air channel interface with film flow of water in a proton exchange membrane fuel cell. *Journal of Power Sources* 2016;302:331–42. <https://doi.org/10.1016/j.jpowsour.2015.10.080>.
- [55] Jo A, Gwak G, Moazzam M, Lee J, Ju H. Analysis of water film formation and low-humidity operation characteristics of a polymer electrolyte fuel cell (PEFC). *International Journal of Hydrogen Energy* n.d. <https://doi.org/10.1016/j.ijhydene.2016.10.014>.
- [56] Rodosik S, Poirot-Crouvezier J-P, Bultel Y. Impact of humidification by cathode exhaust gases recirculation on a PEMFC system for automotive applications. *International Journal of Hydrogen Energy* 2019;44:12802–17. <https://doi.org/10.1016/j.ijhydene.2018.11.139>.
- [57] Reshetenko TV, Bender G, Bethune K, Rocheleau R. Systematic study of back pressure and anode stoichiometry effects on spatial PEMFC performance distribution. *Electrochimica Acta* 2011;56:8700–10. <https://doi.org/10.1016/j.electacta.2011.07.058>.
- [58] Hasheminasab M, Kermani MJ, Nourazar SS, Khodsiani MH. A novel experimental based statistical study for water management in proton exchange membrane fuel cells. *Applied Energy* 2020;264:114713. <https://doi.org/10.1016/j.apenergy.2020.114713>.
- [59] Nandjou F, Poirot-Crouvezier J-P, Chandesris M, Bultel Y. A pseudo-3D model to investigate heat and water transport in large area PEM fuel cells – Part 1: Model development and validation. *International Journal of Hydrogen Energy* 2016;41:15545–61. <https://doi.org/10.1016/j.ijhydene.2016.05.117>.
- [60] Nandjou F, Poirot-Crouvezier J-P, Chandesris M, Rosini S, Hussey DS, Jacobson DL, et al. A pseudo-3D model to investigate heat and water transport in large area PEM fuel cells – Part 2: Application on an automotive driving cycle. *International Journal of Hydrogen Energy* 2016;41:15573–84. <https://doi.org/10.1016/j.ijhydene.2016.06.007>.
- [61] Tsotridis G, Pilenga A, De Marco G, Malkow T, European Commission, Joint Research Centre. EU harmonised test protocols for PEMFC MEA testing in single cell configuration for automotive applications. Luxembourg: Publications Office; 2015.

- [62] Argonne National Laboratory Report # ANL/ESD-18/12. Technology Assessment of a Fuel Cell Vehicle: 2017 Toyota Mirai 2017.
- [63] S++ Simulation Services n.d. <http://www.splusplus.com/measurement/en/csclin.html> (accessed June 7, 2020).
- [64] Fontana M, Ramos R, Morin A, Dijon J. Direct growth of carbon nanotubes forests on carbon fibers to replace microporous layers in proton exchange membrane fuel cells. *Carbon* 2021;172:762–71. <https://doi.org/10.1016/j.carbon.2020.10.049>.
- [65] Robin C, Gérard M, Quinaud M, d'Arbigny J, Bultel Y. Proton exchange membrane fuel cell model for aging predictions: Simulated equivalent active surface area loss and comparisons with durability tests. *Journal of Power Sources* 2016;326:417–27. <https://doi.org/10.1016/j.jpowsour.2016.07.018>.